PROCEEDINGS OF SCIENCE

Level structure of ^{21}Mg: Nuclear and astrophysical implications.

Alexander St J Murphy*
University of Edinburgh
E-mail: a.s.murphy@ed.ac.uk

on behalf of the TUDA collaboration

Resonant elastic scattering of a radioactive ^{20}Na beam incident upon protons in a polyethylene target has been used to probe the level structure of ^{21}Mg above the proton decay threshold. Three states have been observed and their properties deduced through analysis based on the *R*-Matrix formalism. The results improve and extend previous studies of this nucleus. An estimate of the ^{20}Na(p,γ)^{21}Mg reaction rate, including these new data, suggests this reaction will not play a significant role in explosive hydrogen burning in astrophysical sites such as novae and X-ray bursts.

International Symposium on Nuclear Astrophysics — Nuclei in the Cosmos — IX
June 25-30 2006
CERN, Geneva, Switzerland

*Speaker.

PoS(NIC-IX)146

1. Introduction

Little is known about the level structure of the radionuclide ^{21}Mg, or indeed any of the other $T_z = \frac{3}{2}$ *sd*-shell nuclei. Therefore, even at relatively low excitation energies, new data provide important tests of nuclear models and shell structure in this region. Moreover, these nuclei may lie along the path of nucleosynthesis that occurs in accretion driven explosive hydrogen burning, thought to occur in evolved binary systems such as novae and X-ray bursters. It is the energy released by the nuclear reactions that drives the explosions, thus modelling these phenomena requires that the nuclear reaction rates involved be known. The reaction pathways involve resonant proton- and alpha-capture reactions (as well as beta decays) but intrinsic cross sections are small, hampering direct measurements. Since these rates are dominated by resonant processes, an alternative approach is to calculate the reaction rate using detailed knowledge of nuclear states. Such is the motivation for this determination of ^{21}Mg level structure through measurement of the ^{20}Na(^{1}H,^{1}H)^{20}Na resonant scattering reaction in inverse kinematics.

2. Experimental Details and analysis

The experiment was performed at the ISAC TRIUMF facility in Vancouver, Canada [1], using the TRIUMF-UK Detector Array. A driver beam of 20μA of 500 MeV protons was impinged upon a primary silicon-carbide target and a secondary radioactive beam of $^{20}Na^{5+}$ extracted. Up to 5x10^7 pps were post-accelerated, bunched, and made incident upon polyethylene (CH_2) foils of thickness 800 ± 80 μg/cm^2 (provided by the CRC, Louvain-la-Neuve) at energies of 25 and 32 MeV. Elastically scattered protons were detected in 300 μm thick Micron Semiconductors Limited type YY1 silicon strip detectors of the Louvain-Edinburgh Detector Array [2].

The technique of resonant elastic scattering was utilised, in which a heavy-ion projectile loses a significant fraction of its energy in passing through a thick target. Elastic scattering occurring at different target depths corresponds to a wide range of centre-of-mass reaction energies: proton energy spectra may then be interpreted as excitation functions. Excited states in a compound nucleus manifest themselves as resonances built upon a Rutherford scattering background with a shape determined by the nuclear properties of state (excitation energy, spin, angular momentum transfer) plus any interference effects. *R*-matrix analysis [3, 4] allows extraction of these properties in a (near) model independent way.

A schematic diagram of the apparatus used is shown in Figure 1. Two LEDA arrays were used covering laboratory angles of 14.4°–33.7° and 4.7°–12.1°. Mylar sheeting was used to protect the detectors from radiation damage induced by the high flux of elastically scattered beam particles. The energy loss incurred by protons exiting the target and passing through the Mylar sheeting and detector dead-layer, although small, was corrected for in all data analysed. One sector on the near-to-target detector was left unshielded to provide on-line diagnostics. Unfortunately, the detector viewing larger laboratory scattering angles could not used in subsequent *R*-matrix analysis due to calibration problems. A high precision pulser was used to determine ADC offsets and linearities, while the LEDA detectors were calibrated using of a standard triple-alpha source. The typical resolution of the alpha peak at 5.486 MeV was 31 keV FWHM for a single detector element. In

subsequent analysis the energy calibration was modified to include the well known pulse height defect for alpha particles relative to protons [5].

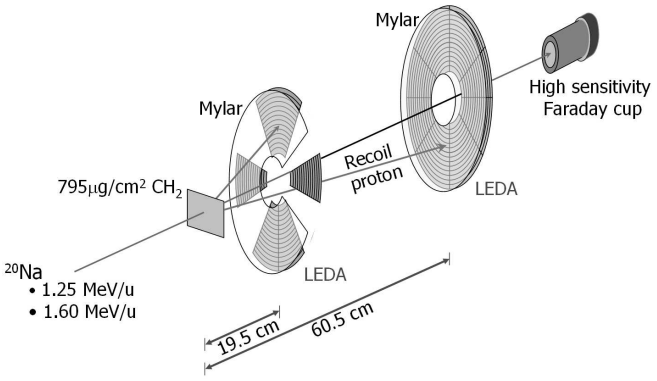

Figure 1: Schematic diagram of the experimental apparatus employed at the TUDA facility.

Figure 2 shows a plot of the energy of detected particles (in the laboratory frame) vs. time-of-flight for all data taken at the 1.600 MeV/u (32 MeV lab) beam energy setting and scattered into the annulus of detector elements located at a polar angle of 5.3°. The vertical bands are caused by beta-delayed alpha-particle decay of ^{20}Na ions that have stopped in the protective Mylar sheets. Elastic scattering of the ^{20}Na beam from carbon atoms in the target occurs at a relatively high centre-of-mass energy, resulting in some recoiling carbon ions having sufficient energy to escape the Mylar foils. These events are seen as the lower of the curved loci seen in Figure 2. The final well-separated locus corresponds to the events of interest; elastically scattered protons.

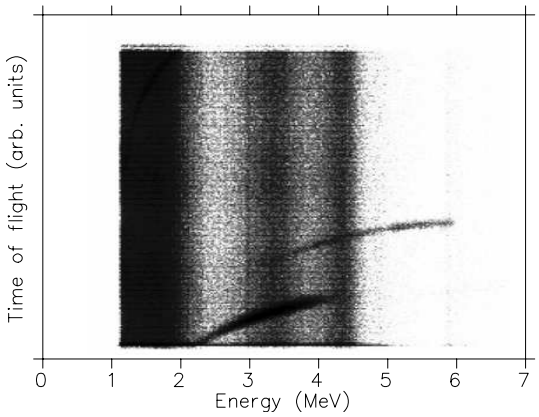

Figure 2: Plot of laboratory energy versus time-of-flight for all particles detected at 5.3 ° for the 1.600 MeV/u beam energy data set. See text for details.

The data acquisition was operated such that the time-to-digital converters (TDCs) started on the detection of a particle, and stopped on the next accelerator RF signal. Thus faster moving ions have larger TDC conversions. Additionally, the use of leading edge discriminators in the timing of the start signal means that signals of larger amplitude start earlier. These combined effects lead to the shape of the locus observed. A suitable algorithm applied to the TDC signal allows

Table 1: Energy, proton decay and reduced widths for states in ^{21}Mg, obtained from the present data.

Resonance 1				Resonance 2				Resonance 3			
J	E (keV)	Γ_p (keV)	γ_c (MeV$^{1/2}$)	J	E (keV)	Γ_p (keV)	γ_c (MeV$^{1/2}$)	J	E (keV)	Γ_p (keV)	γ_c (MeV$^{1/2}$)
$\frac{3}{2}$	780	8±3	0.86	$\frac{5}{2}$	1002	5^{+4}_{-2}	0.29	$\frac{3}{2}$	1312	65±8	0.69

these effects to be removed and thus the proton locus linearised. A simple software cut may then be implemented to select the region corresponding to the elastically scattered protons, as well as nearby regions which determine the alpha decay background.

Figure 3 shows the background subtracted proton energy spectra obtained. Clearly, three strong resonances are observed, at centre-of-mass energies close to 780, 1000 and 1320 keV. These data have been analysed within the *R*-matrix formalism in order to extract further information. A χ^2 minimisation technique revealed unambiguously that all three resonances are populated through ℓ=0 angular momentum transfer, and given that the ground state spin of ^{20}Na is 2^+, this implies the states being populated must be of either $J^\pi=\frac{3}{2}^+$ or $\frac{5}{2}^+$ character. The *R*-matrix analysis was able to strongly suggest that both the lowest and highest resonances correspond to states in ^{21}Mg with $J^\pi=\frac{3}{2}^+$. Further comparison with an *sd*-shell shell model calculation conducted using the OXBASH [6] code employing the Wildenthal USD interaction, and with well established $T=\frac{3}{2}$ states in the neighbouring $T_z=\frac{1}{2}$ ^{21}Ne and ^{21}Na nuclei, allows the state in ^{21}Mg corresponding to the resonance located near 1000 keV to be assigned a $J^\pi=\frac{5}{2}^+$. The location, spins and proton decay widths of the states seen are summarised in Table 1.

3. Astrophysical Implications

Under the assumption of isolated narrow resonances, the stellar reaction rate per particle pair may be calculated. For a H density typical of novae, the contributions of each of the states known to exist in ^{21}Mg are shown in Figure 4. The inclusion of the new data is of little impact. Consequently, these data add to the view that rp-process breakout from the hot CNO cycle is very unlikely to proceed through the ^{15}O(α,γ) ^{19}Ne(p,γ) ^{20}Na(p,γ) ^{21}Mg reaction sequence, at least in novae and X-ray bursters.

References

[1] R.E. Laxdal, Nucl. Instrum. Meth. B **204** (2003) 400

[2] T. Davinson *et al.*, Nucl. Instrum. Meth. A **454** (2000) 350

[3] R.G. Thomas, Phys. Rev. **88** (1952) 1109

[4] A.M. Lane and R.G. Thomas, Rev. Mod. Phys. **30** (1958) 257

[5] D.J. Skyrme, Nucl. Instrum. Meth. **57** (1967) 61

[6] *Oxbash for Windows*, B.A. Brown, *et al.* MSU-NSCL report number 1289 (2004).

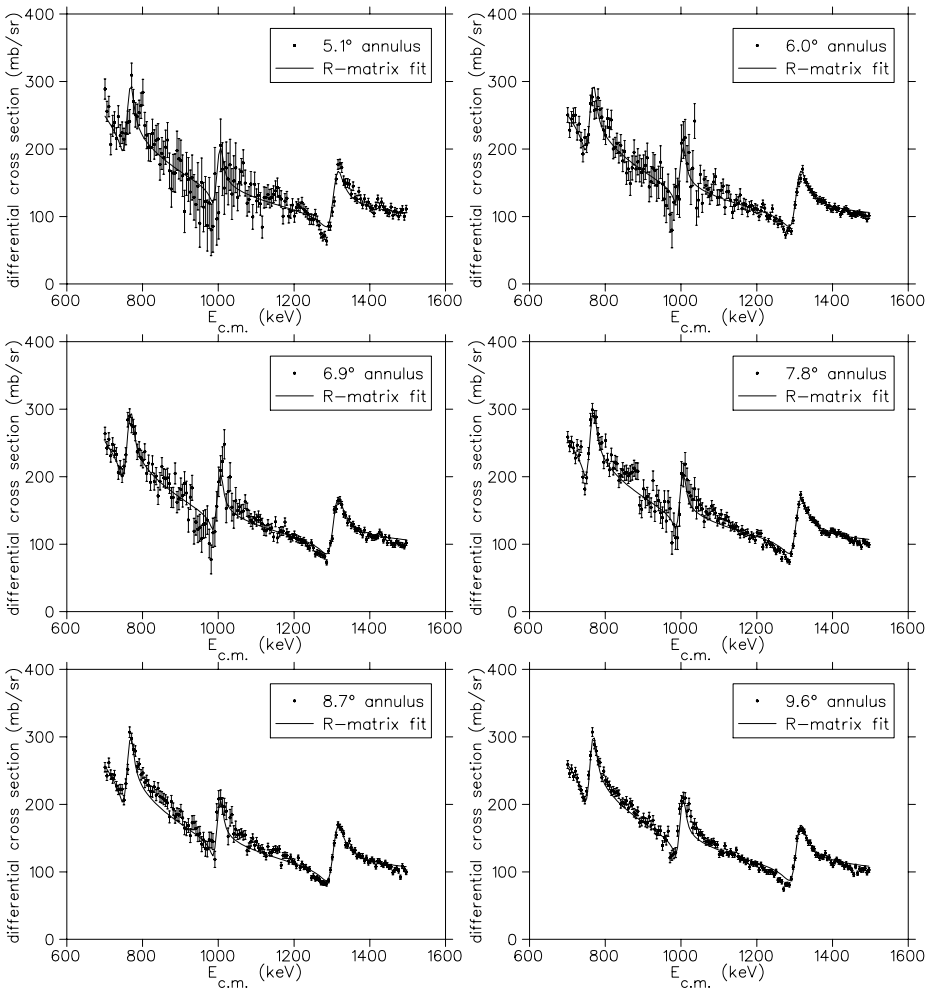

Figure 3: Global *R*-matrix fit assuming the states in ^{21}Mg which have, $J = \frac{3}{2}$, $\frac{5}{2}$ and $\frac{3}{2}$ and are populated by *s*-waves. Pairs of LEDA annuli have been summed to improve statistics. Error bars on data points reflect statistical uncertainties only.

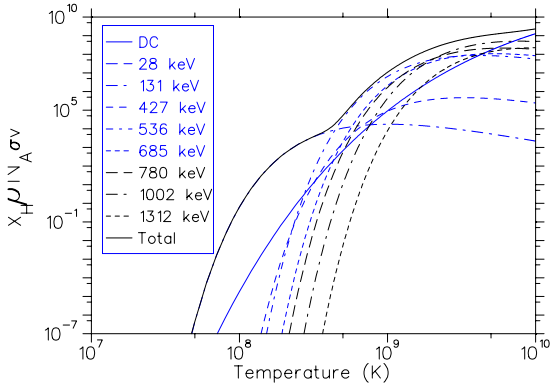

Figure 4: Contributions of various states in ^{21}Mg to the ^{20}Na(p,γ)^{21}Mg reaction rate, together with the total reaction rate calculated as the linear sum of contributions.